ACS OMEGA

http://pubs.acs.org/journal/acsodf

Article

High Compression Ratio Active Pre-chamber Single-Cylinder Gasoline Engine with 50% Gross Indicated Thermal Efficiency

Wenfeng Zhan, Hong Chen, Jiakun Du,* Bin Wang, Fangxi Xie, and Yuhuai Li

Cite This: *ACS Omega* 2023, 8, 4756−4766

Read Online

ACCESS | Metrics & More | Article Recommendations

ABSTRACT: Active pre-chamber turbulent jet ignition with a high compression ratio has been demonstrated to be an effective method for significantly enhancing engine thermal efficiency. A dual modification of the combustion chamber and the pre-chamber was performed on an AVL 5400 single-cylinder Miller engine to achieve stable ultra-lean burn at a high compression ratio, and a breakthrough of 51.10% gross indicated thermal efficiency was achieved at the compression ratio of 16.4 and λ = 2.236. Spark ignition and pre-chamber turbulent jet ignition exhibit significant performance diversities under lean burn conditions. Pre-chamber turbulent jet ignition is able to significantly expand the lean burn limit of spark ignition to λ = 2.7 (CoV_{IMEP} < 5%) at only the expense of an increased HC emission, while apparently reducing fuel consumption and nitrogen oxide emissions. With an increase in the compression ratio from 13.6 to16.4, spark ignition and pre-chamber turbulent jet ignition exhibit contradictory performance laws. The engine performance of a spark ignition engine decreases significantly as the compression ratio increases, whereas a pre-chamber jet ignition engine can still operate reliably at a high compression ratio with ultra-lean combustion. Within the scope of the test, the performance of the pre-chamber jet ignition engine is enhanced by a greater compression ratio. This improvement is primarily attributable to the reduction of heat transfer loss and exhaust energy loss under ultra-lean combustion, as determined by an analysis of the structure of power losses.

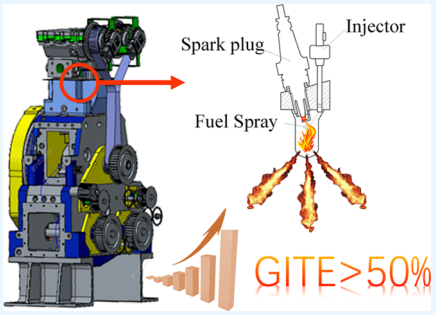

1. INTRODUCTION

With the frequent occurrences of extreme weather, it is imperative that transportation systems conserve energy and reduce emissions. Extended-range electric vehicles are considered a promising technology for the future development of engines.[1] In this technology, the engine is viewed as a generator and only needs to be operated under ideal conditions to maximize fuel efficiency.[2,3]

The lean burn technology is considered one of the most important means to improve the engine's thermal efficiency in specific operating conditions.[4,5] On one hand, lean burn means more fresh air into the cylinder, increasing the frequency of fuel−air contact and making the fuel burn more completely. On the other hand, lean burn reduces the pumping loss and heat transfer loss of the engine, further improving thermal efficiency.[6,7] The leaner charge can achieve better fuel economy and emission performance, but it requires more ignition energy and a faster flame propagation speed to maintain stable combustion.[8]

Mixture stratification and high-energy ignition are two strategies for extending the lean limit of an engine. Gong et al. have significantly increased the lean burn limit of methanol engines using the stratified lean burn technology, while simultaneously improving thermal efficiency and decreasing pollutant emissions.[9] Dongwon Jung et al. successfully extended the lean burn limit of spark ignition engines from 1.5 to 1.81 through the ultra-high energy ignition strategy of multiple ignition coils. Additionally, coupling with the high tumble ratio technology, they successfully extended the stable lean burn condition to λ = 1.9 and obtained a 16.5% indicated thermal efficiency improvement.[10]

Although these strategies can significantly improve the lean burn performance of the engine, they still have technical defects in practical application. For example, the spark plug would be eroded with high-energy ignition system due to the higher electrode temperature.[11] In addition, lower flame propagation should be a critical factor for lean burn performance, which lead to inconspicuous improvement on thermal efficiency under ultra-lean burn conditions.[12] Pre-chamber turbulent jet ignition is a technique that simultaneously employs these two lean burn limit expansion strategies.[13] This technology replaces the spark plug in a conventional spark ignition engine with a pre-chamber.[14] When the engine requires ignition, the injector in the pre-

Received: October 22, 2022
Accepted: December 27, 2022
Published: January 29, 2023

chamber enriches the lean mixture in the pre-chamber, followed by the ignition of the spark plug in the pre-chamber.[15] After establishing the pressure difference between the pre-chamber and the main combustion chamber,[16,17] the high-temperature combustion products are injected into the main chamber as hot jets through the pre-combustion chamber nozzle, igniting the lean mixture in the cylinder with extremely high ignition energy.[18,19]

The lean burn performance of turbulent jet ignition natural gas engines was investigated by Zhao et al. Active turbulent jet ignition can extend the lean burn limit to 2.1 and achieve a maximum indicated thermal efficiency of 45 %, according to the study. Exhaust gas recirculation dilution can reduce THC emissions by up to 78% under lean burn conditions.[20] By utilizing the pre-chamber technology, Hua et al. were able to achieve ultra-lean burn in spark ignition engines. They discovered that using the pre-chamber technology, NOx emissions were reduced by more than 95%, and the combustion instability of the engine was reduced under lean combustion conditions.[21] Michael et al. compared spark ignition and pre-chamber turbulent jet ignition engine performances. The study found that under ultra-lean conditions, the use of turbulent jet ignition can reduce the brake-specific fuel consumption (BSFC) by 20−25%, bringing the engine BSFC closer to 200 g/kWh.[22] Attard et al. configured an active pre-chamber on a light-duty gasoline engine with a compression ratio of 10.4.[23−25] The study showed that the maximum engine efficiency was increased by more than 20% compared with that of spark ignition, and the peak indicated that the thermal efficiency reached 42.8%. In addition, the pre-chamber turbulent jet ignition also has a suppressing effect on knocking.[26] According to this characteristic, Shah et al. carried out the pre-chamber modification of the heavy-duty diesel engine, changed the compression ratio to 12, realized ultra-lean burn with a lambda of 2.4, and increased the gross indicated thermal efficiency (GITE) to 47.6%.[27]

A high compression ratio with an active ultra-lean burn pre-chamber turbulent jet ignition system is a novel concept for increasing the engine's maximum thermal efficiency. In light of this, this paper investigates the thermal efficiency limit of gasoline engines with an active pre-chamber at ultra-high compression ratios. Also, a series of comparative tests with the performance of spark ignition engines under a high compression ratio are conducted to provide a reference for the future ultra-high thermal efficiency engine development process.

2. EXPERIMENTAL SETUP AND METHODS

2.1. Experimental Setup. The tests were conducted on an AVL 5400 Miller cycle research single-cylinder engine. The bore and stroke are 79 and 102 mm respectively. Table 1 provides additional information about the experimental engine. A programmable control unit controls fuel injection and ignition in the engine. By replacing the gasket between the cylinder head and cylinder block, the compression ratio of the engine can be adjusted. Notably, the volume of the pre-chamber increases the volume of the combustion chamber. The compression ratio of pre-chamber turbulent jet ignition is slightly lower than that of spark ignition for the same combustion chamber. In this paper, the compression ratio comparison is based on the pre-chamber turbulent jet ignition. Under spark ignition, the actual compression ratios for compression ratios of 13.6, 14.5, and 15.4 are 13.94, 14.8, and 15.8, respectively.

Figure 1 and Table 2 depict the engine test platform's schematic diagram and equipment parameters, respectively.

Table 1. Engine Parameter

engine parameter	specification
engine type	single cylinder research engine
engine parameter	DOHC, GDI, four-valve, four-stroke, single cylinder
Bore × Stroke/mm	79 mm × 102 mm
displacement	0.5 L
comprehension ratio	13.6, 14.5, 15.4, 16.4

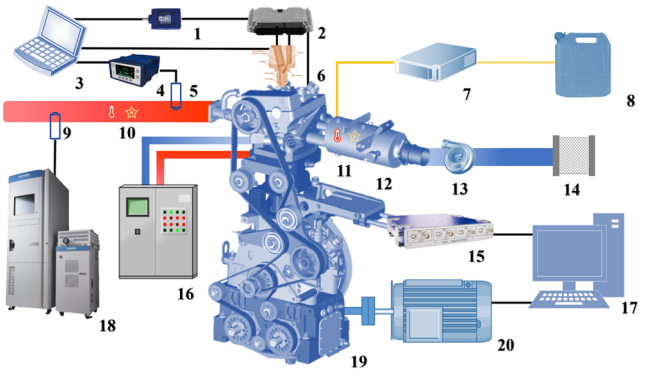

Figure 1. Schematic diagram of the test system. 1: USB-CAN, 2: ECU, 3: INCA system 1, 4: lambda meter, 5: lambda meter probe, 6: pre-chamber system, 7: fuel flow meter, 8: fuel tank, 9: exhaust analyzer probe, 10: exhaust temperature and pressure sensor, 11: intake temperature and pressure sensor, 12: intake heater, 13: intake supercharge system, 14: air filter, 15: AVL combustion analyzer, 16: engine coolant system, 17: AVL system, 18: HORIBA MEXA-7500D, 19: AVL 5400 single cylinder research engine, and 20: dynamometer.

Table 2. Main Measurement Devices' Specifications and Parameters

equipment	model	accuracy
dynamometer	ACWA-100 5-4-290	torque: ±0.03% speed: ±1 rpm
pressure sensor	KISTLER 6054BR	±0.3%
combustion analyzer	AVL INDIMCRO 602	
crank angle encoder	AVL 365C	±0.5°
intake supercharging system	AVL 515	±50 mbar
thermostatic unit	AVL 577	±1 °C
fuel flow meter	AVL 7361 CST	±0.05%
exhaust gas analyzer	HORIBA MEXA-7500D	calibration check: ±0.5% repeatability test: ±0.5%

The AVL515 system was used to supercharge the engine's intake air during the test. A transient dynamometer from AVL is utilized to measure and control the engine's output power. The AVL 7361 CST, ETAS ES630, and AVL Indicom combustion analyzers gathered information on the fuel consumption rate, lambda, and engine cylinder pressure. The AVL 577 thermostatic control unit maintains a constant temperature for the engine oil and the cooling water. HORIBA MEXA-7500D is utilized in the experiment to analyze exhaust gas components. It is a high-precision and rapid-response

https://doi.org/10.1021/acsomega.2c06810
ACS Omega 2023, 8, 4756−4766

emission analysis device created by HORIBA in Japan. It has the ability to analyze CO, CO_2, O_2, THC, and NO_x in the engine exhaust gas.

2.2. Design of the Pre-Chamber. Figure 2 is a schematic diagram of the structure of the pre-chamber, and Table 3

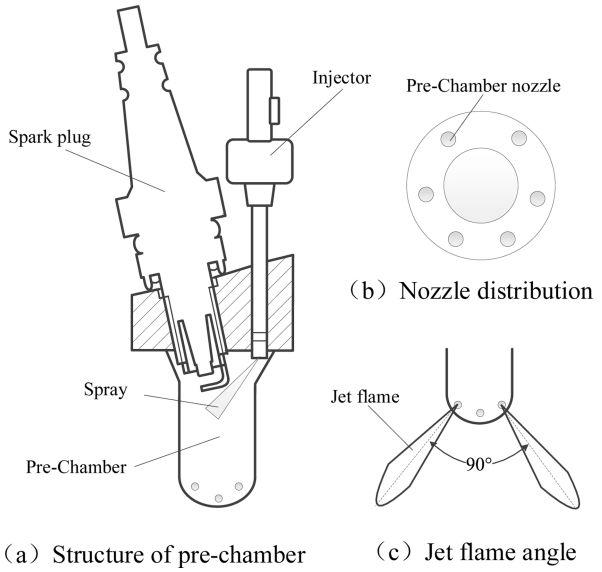

Figure 2. Schematic diagram of the pre-chamber.

Table 3. Pre-Chamber Parameter

pre-chamber parameter	specification
pre-chamber volume	1.7 mL
fuel injection pressure	10 MPa, DI
pre-chamber type	active pre-chamber
pre-chamber cooling method	water cooling
number of nozzles	6
diameter of the nozzle	1.2 mm
jet angle	90°

shows the specific structural parameters of the pre-chamber. The volume of the pre-chamber is approximately 1.7 mL, and it has six nozzles with a diameter of 1.2 mm and a 90° axis angle between adjacent nozzles. The pre-chamber is equipped with independent fuel injection systems, a laser-welded single-hole injector mounted on the top of the pre-chamber with the spark plug. The injector is oriented as depicted in Figure 2, and the angle between the direction of the spray plume and the injector axis was 30°. To make the turbulent jet of each pre-chamber nozzle more uniform, the pre-top chamber's structure is asymmetric, and the spark plug electrode is positioned roughly in the top center of the pre-chamber. The upper portion of the pre-chamber is cooled by the engine's water jacket, preventing it from overheating.

The timing of the pre-chamber injection was calibrated prior to the engine experiment. The optimal pre-chamber injection timing for the current pre-chamber configuration is 90° bTDC. Previous work has evaluated the amount of fuel injected prior to the chamber.[17] In this study, the pre-chamber fuel injection pressure is 10 MPa, the injection pulse width is 0.25 milliseconds, and the fuel injection amount is about 0.353 mg. During the test, the corresponding main combustion chamber and pre-chamber fuel ratio is 6 ± 0.5%, which is slightly higher than the ratio of the volume of the pre-chamber to the main chamber (4.93%, CR = 14.5).

2.3. Operation Conditions. This paper investigates the optimal expansion of the engine's thermal efficiency. Throughout the test, all test points are operated at the engine's global optimal efficiency point (RPM: 2750 rpm and IMEP: 10.50 bar). During the test, the ignition timing of each test point corresponds to the minimum advance for the best torque (MBT) for the optimal torque angle under the current operating conditions. Due to the high compression ratio of the engine in this test, knocking is very likely to occur under certain operating conditions; consequently, the ignition timings are retarded to the maximum spark timing that can occur without knocking. To make the test results more applicable, China southern commercial RON 92 gasoline with a measured calorific value of 42.237 MJ/kg was used as the test fuel. The engine's main chamber and pre-chamber are supplied by two independent fuel supply systems. In the main chamber, the injection pressure was 35 MPa, while in the pre-chamber, it was 10 MPa. The injection timing in the primary combustion chamber is 300° bTDC. The temperature of the engine oil was maintained at 90 ± 2 °C using the circulating water system.

To improve the accuracy and repeatability of the test, 200 consecutive cycles of cylinder pressure data were taken at each experimental point under the condition of stable torque. These cylinder pressure data are used to calculate and analyze the engine performance. The engine performance data was calculated using the AVL Indicom combustion analyzer. The fast formula calculated the heat release rate with a constant adiabatic coefficient, and the engine cycle-to-cycle variation coefficient was presented by CoV_{IMEP}, which was limited to less than 5%.

2.4. Power Loss Estimation Method. This test evaluates the energy balance of the engine using the following estimating method.[28]

The energy generated by fuel combustion is finally divided into five parts: effective work, exhaust energy, heat transfer energy, friction work, and unburned energy. This study focuses primarily on the energy loss component, which corresponds to pumping loss, heat transfer loss, friction loss, unburned loss, and exhaust loss.

The formula for calculating the total chemical energy power of the fuel is

$$P_{Fuel} = \frac{R_{Fuel} \times LHV_{Fuel}}{3.6} \quad (1)$$

LHV_{Fuel} is the low heat value of gasoline (MJ/kg), whereas R_{Fuel} represents the fuel consumption per unit time (kg/h). The low calorific value of gasoline measured in this test is 42,237 MJ/kg.

The engine's unburned losses are primarily of incomplete oxidation of THC, CO, and NO. For this test, the amount of NO cannot be measured; therefore, this calculating technique focuses on the unburned portion of THC and CO, using the following estimation formula

$$P_{UbL} = \frac{M_{THC} \times LHV_{THC} + M_{CO} \times LHV_{CO}}{3600} \quad (2)$$

M_{THC} and M_{CO} represent the emission flow rates (g/h) of THC and CO, while LHV_{THC} and LHV_{CO} represent the lower heat values (MJ/kg) of THC and CO, respectively.

The pumping loss estimation formula is

https://doi.org/10.1021/acsomega.2c06810
ACS Omega 2023, 8, 4756−4766

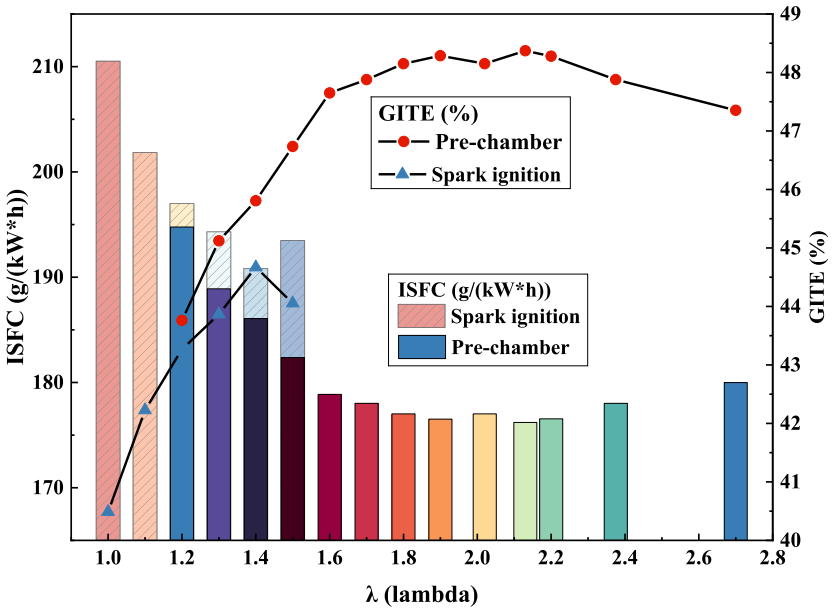

Figure 3. Economic comparison between spark ignition and pre-chamber turbulent jet ignition under different lambdas.

$$P_{PL} = \frac{V \times 0.5 \times \text{IMEPL} \times \text{Speed}}{600} \quad (3)$$

where V is the engine displacement, IMEPL is the mean indicated pressure at low pressure, and Speed is the engine speed.

The friction loss estimation method is

$$P_{FL} = \frac{V \times 0.5 \times (\text{IMEP} - \text{BMEP}) \times \text{Speed}}{600} \quad (4)$$

where IMEP is the mean indicated pressure and BMEP is the mean effective pressure.

The power carried in the intake and exhaust are, respectively,

$$P_{In} = \frac{Cp_{In} \times (T_{In} - 20) \times M_{In}}{3.6 \times 10^6} \quad (5)$$

$$P_{Ex} = \frac{Cp_{Ex} \times (T_{Ex} - 20) \times M_{Ex}}{3.6 \times 10^6} \quad (6)$$

Cp_{In} and Cp_{Ex} represent the intake and exhaust constant-pressure specific heat capacities (J/kg·K), respectively, while T_{In} and T_{Ex} represent the intake and exhaust temperatures (°C), respectively. M_{In} and M_{Ex} are the intake and exhaust mass flow rates (kg/h), respectively.

The heat transfer in the cylinder is ultimately lost in the form of the coolant, oil, and radiation heat transfer, and hence, it cannot be monitored directly. This research estimates the heat release loss by removing other power losses from the total chemical energy power of fuel. The precise procedure is as follows

$$P_{HL} = P_{Fuel} + P_{In} - (P_e + P_{FL} + P_{PL}) - P_{Ex} - P_{UbL} \quad (7)$$

P_e is the effective power output by the engine.

3. RESULTS AND DISCUSSION

3.1. Influence of the Pre-Chamber Turbulent Jet Ignition System on Engine Combustion and Emission Performance. In this section, the compression ratio of the engine is set to 14.5, and a lean burn limit scan of spark ignition and pre-chamber turbulent jet ignition is performed. The particular test results are displayed below.

Figure 3 depicts the lean limits for spark ignition and pre-chamber turbulent jet ignition at various excess air ratios, as well as the GITE and the indicated specific fuel consumption (ISFC) for various lambdas. The transformation law of efficiency of spark ignition and pre-chamber ignition is relatively similar as lambda increases: efficiency gradually increases and then decreases. The lean limit of spark ignition is approximately lambda = 1.5, whereas adding a pre-chamber appears to extend the lean limit to approximately lambda = 2.7, while maintaining stable engine operation. The active pre-chamber additionally enhances the engine's optimal lean burn operating point. The optimal operating lambda of a conventional spark ignition engine is approximately 1.4, but the active pre-chamber can increase it to 2.1. This represents a substantial improvement over the pre-chamber expansion lean limit reported in the previous literature.[17] The maximum GITE of turbulent jet ignition in the pre-chamber is 48.37% (lambda = 2.13), and the corresponding ISFC is 176.20 g/kWh. The maximum GITE of spark ignition is 44.67% (lambda = 1.4), and the ISFC is 190.81 g/kWh.

The expansion of the lean burn limit by the pre-chamber turbulent jet ignition is the optimization of the combustion process by the pre-chamber turbulent jet, as illustrated in Figure 4. When lambda is greater than 1.3, the combustion process of spark ignition is considerably prolonged. Both spark ignition and flame propagation are significantly inhibited by the mixture's reduced flammability. For the pre-chamber turbulent jet ignition, the spark plug is guarded in the pre-chamber. Even in the ultra-lean burn condition, the injector in the pre-chamber enriches the charge in the pre-chamber separately. Thus, the pre-chamber mixture is always in a highly flammable concentration. In addition, the pre-chamber turbulent jet carries a great deal of energy and active radicals, which facilitates ignition. Even under the ultra-lean burn condition ($\lambda > 2.0$), the combustion duration of pre-chamber turbulent jet ignition is still shorter than that of spark ignition's

https://doi.org/10.1021/acsomega.2c06810
ACS Omega 2023, 8, 4756−4766

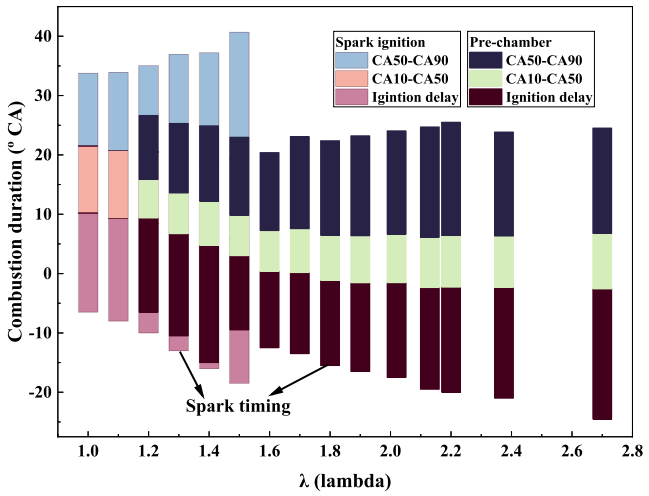

Figure 4. Combustion process comparison between spark ignition and pre-chamber turbulent jet ignition under different lambdas.

stoichiometric combustion. In addition, Figure 4 demonstrates that the active pre-chamber performs poorly under the mild lean burn condition. This is due to the fact that even a small amount of enrichment of the pre-chamber mixture will result in an overly rich pre-chamber mixture under mild lean combustion, which will greatly increase the formation time of the fire core in the pre-chamber and subsequently affect the ignition delay in the main chamber.

For a comprehensive examination of the distinction between spark ignition and pre-chamber turbulent jet ignition, Table 4 compares five typical operating cases. Figure 5 illustrates the pressure, heat release rate, and temperature variation under typical spark ignition and pre-chamber turbulent jet ignition operating conditions. These cases' efficiency and power loss are depicted in Figure 6. Comparing case 1 to case 2, the combustion center of case 1 is relatively lag. In case 2, although the peak cylinder pressure is higher and the cylinder pressure curve is relatively smooth, the peak heat release rate is significantly lower, and the heat release process is lengthier, as depicted in Figure 5b. Due to the low ignition energy of spark ignition, it is difficult to form fire kernel under conditions of lean combustion. Although increasing the ignition advance angle can move the combustion center of gravity forward, the scarcely formed fire nuclei have a tiny ignition area, so the exothermic reaction takes a very long time (Figure 5b). Although the unburned loss and heat transfer loss are reduced, it appears that the beneficial effect is limited (Figure 6b).

When the case3 ignition mode is replaced with the pre-chamber turbulent jet ignition, the peak cylinder pressure is significantly increased, the heat release rate and the in-cylinder temperature are increased, and the combustion process is shortened considerably. As shown in Figure 6a, the changes in the cylinder pressure, heat release rate, and cylinder temperature ultimately improved the engine efficiency. Even under ultra-lean burn circumstances, the turbulent jet ignition in the pre-chamber has a larger ignition area and improves the turbulent kinetic energy in the main combustion chamber, allowing for an effective heat release process. On one hand, the increased intake air further reduces the engine's pumping loss (the engine used in the test is a Miller engine, and the initial pumping loss is low). On the other hand, it increases the frequency of contact between fuel and air so that the fuel burns more completely, thereby reducing unburned losses significantly.

Comparing cases 3−5, it can be found that the cylinder pressure gradually increases with the increase of lambda. Even when the engine runs at a high compression ratio, ultra-lean burn never faces the knocking, so the spark time can be greatly advanced for higher engine efficiency. From Figure 5b, when lambda is increased from 2.13 to 2.7, the engine heat release rate does not change significantly, and the change in cylinder pressure is mainly caused by the difference in intake pressure. In addition, the cylinder temperature gradually decreases with the lambda increase, which corresponds to the stepwise reduction in heat transfer losses in Figure 6b. It is worth noting that operating at leaner conditions can significantly reduce heat transfer losses, and the engine will face challenges of unstable operation and increased unburned losses.

Similar rules govern the evolution of emission data for spark ignition and turbulent jet ignition at various excess air ratios (as shown in Figure 7). Both HC and CO emissions increased with the excess air coefficient ($\lambda \geq 1.2$), and the NOx emission decreased with the excess air coefficient. HC emissions are mainly produced by incomplete combustion. On one hand, an increase in the amount of air results in an increase in the specific heat capacity of the cylinder, where the same amount of heat release will produce a lower temperature increase effect, and as a result, the chemical reaction rate decreases, preventing the HC from being completely oxidized in the limited time available during each engine cycle. On the other hand, the lean charge slows combustion in the cylinder and prevents the flame from reaching the cylinder's edge, resulting in an increase in HC emissions. It is important to note that pre-chamber turbulent jet ignition can result in faster flame propagation (as depicted in Figure 4), which should substantially reduce HC emissions. However, the pre-chamber increases the engine cylinder's clearance volume. Moreover, when the mixture in the main chamber is successfully ignited, the main chamber's cylinder pressure will be higher than that of the pre-chamber, resulting in a reverse jet flow and a large amount of unburned mixture jet into the pre-chamber, which further increases HC emissions.[29] The increase in the excess air coefficient did not result in a significant increase in CO emissions. The production of NOx necessitates primarily high temperatures and oxygen enrichment. Although lean burn provides a large

Table 4. Case Setting

no.	ignition mode	lambda	spark time	main-chamber fuel injection time (°bTDC)	pre-chamber fuel injection time (°bTDC)	pre-chamber fuel injection quantity (mg)
Case 1	spark	1.0	−6.5	−300	−90	0.353
Case 2	spark	1.5	−18.5	−300	−90	0.353
Case 3	jet	1.5	−9.5	−300	−90	0.353
Case 4	jet	2.13	−19.5	−300	−90	0.353
Case 5	jet	2.7	−24.5	−300	−90	0.353

https://doi.org/10.1021/acsomega.2c06810
ACS Omega 2023, 8, 4756−4766

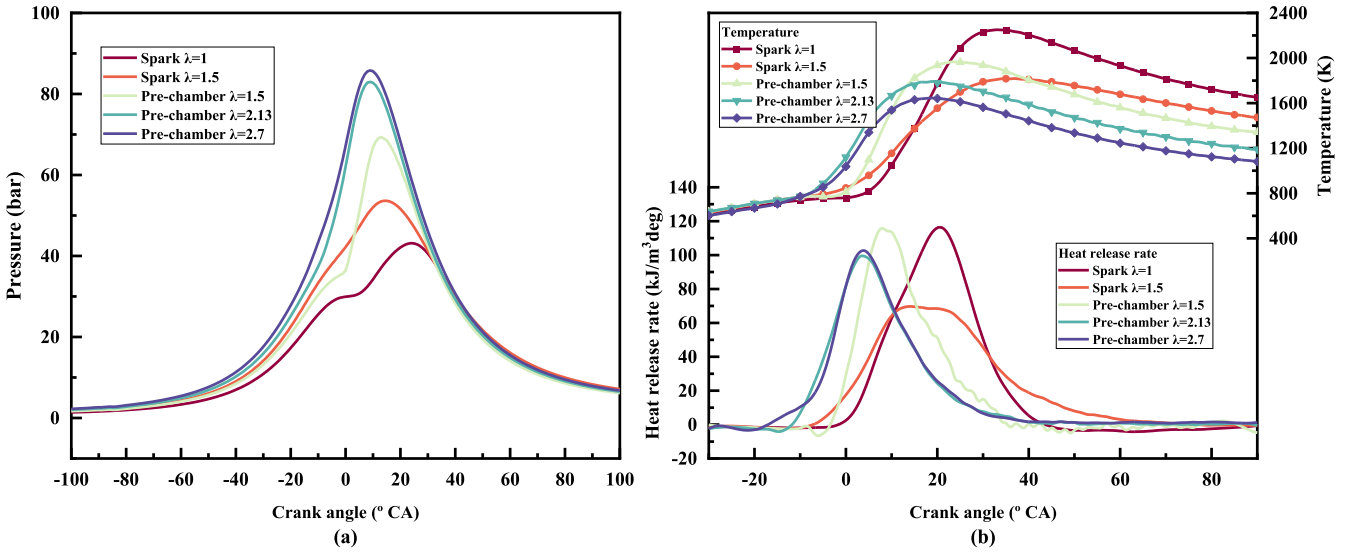

Figure 5. Comparison of spark ignition and pre-chamber turbulent jet ignition: (a) cylinder pressure comparison and (b) temperature and heat release rate comparison.

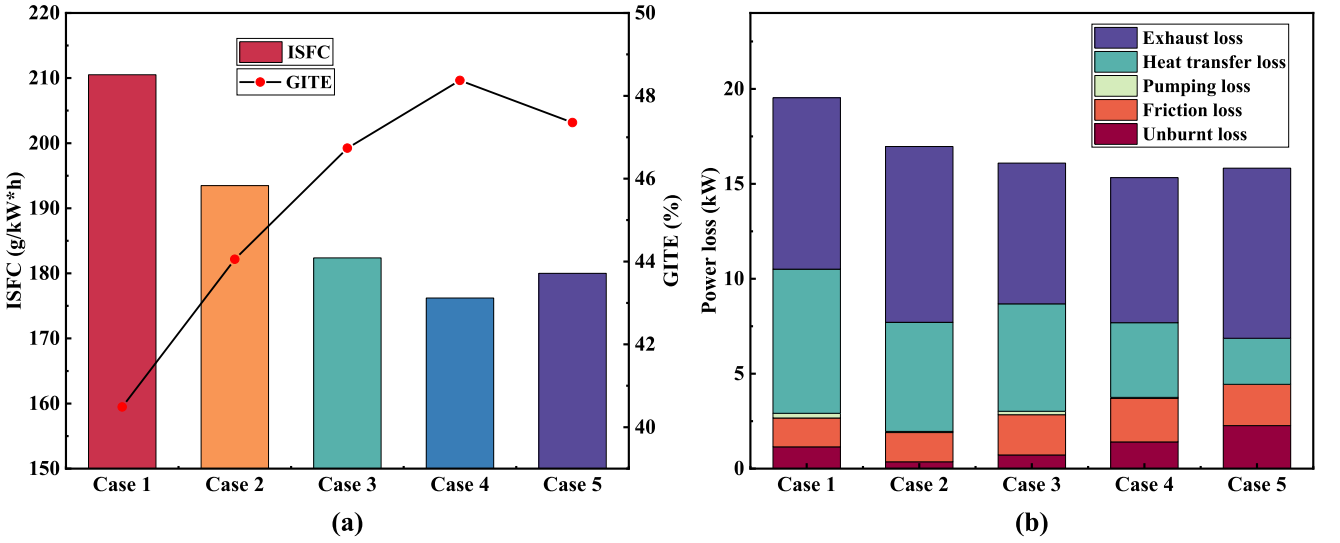

Figure 6. Comparison under typical conditions of spark ignition and pre-chamber turbulent jet ignition: (a) engine economy comparison and (b) engine power loss comparison.

amount of oxygen, the decrease in temperature makes the reaction difficult to proceed and reduces NOx emissions by a large margin.

3.2. Comparative Study on Combustion and Emission of the Compression Ratio on Spark Ignition and in Pre-chamber Turbulent Jet Ignition. Figure 8 depicts the GITE of spark ignition and pre-chamber turbulent jet ignition under varying compression ratios, as well as the ISFC comparison under the optimal compression ratios (spark: 13.6 and pre-chamber: 16.4). Spark ignition and pre-chamber turbulent jet ignition have significantly different compression ratio tolerances. Spark ignition performance degrades with increasing compression ratios, whereas pre-chamber turbulent jet ignition improves. The poor performance of spark ignition at high compression ratios is primarily a result of the knock factor's limitation. Under high compression ratios, MBT must make concessions due to knocking restrictions. The delayed ignition timing causes the overall combustion phase of spark ignition to be delayed, resulting in an increase in heat transfer loss and unburned loss, which reduces performance. The pre-chamber efficiency is drastically enhanced by high compression ratios, particularly under ultra-lean burn conditions. For a pre-chamber turbulent jet ignition with a compression ratio of 16.4, the GITE can reach 51.10% at a lambda of 2.236, which corresponds to an ISFC of 166.78 g/kWh. Compared to the stoichiometric combustion of the original machine (compression ratio: 14.5 and GITE = 40.49%), the GITE improvement is more than 10%.

Table 5 compares the optimal lambda values for various compression ratios. At higher compression ratios, the optimal lambda for turbulent jet ignition in the pre-chamber increases. At high compression ratios, the prechamber's resistance to ultra-lean combustion is increased. The variation of GITE and ISFC for spark ignition and pre-chamber turbulent jet ignition under normal operating conditions is depicted in Figure 9. In conjunction with Table 5, it can be seen that as the compression ratio increases, spark ignition continues to experience knocking under lean burn conditions. Therefore,

https://doi.org/10.1021/acsomega.2c06810
ACS Omega 2023, 8, 4756−4766

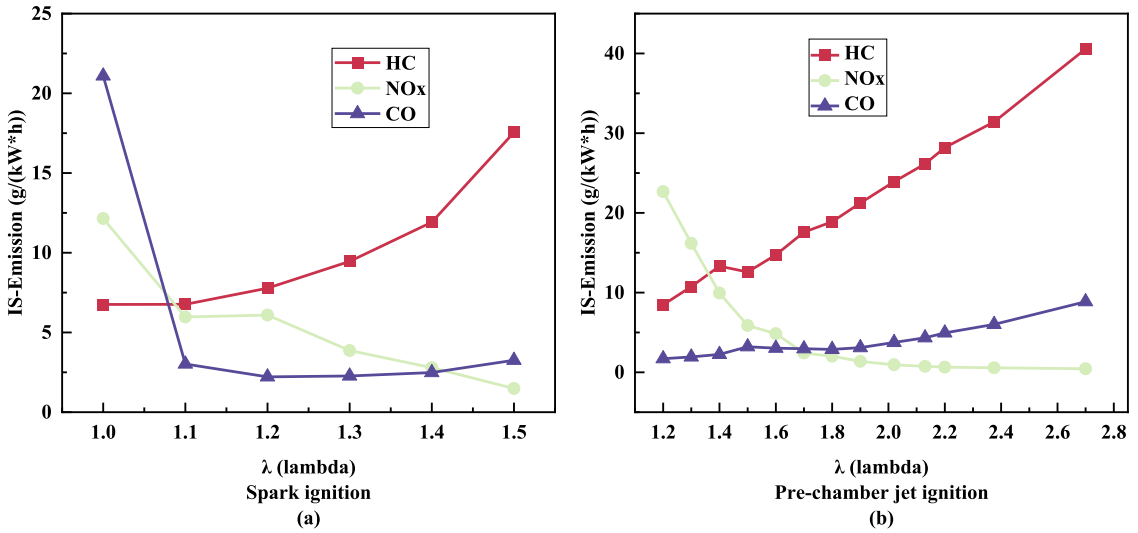

Figure 7. Emission comparison between spark ignition and pre-chamber turbulent jet ignition under different lambdas.

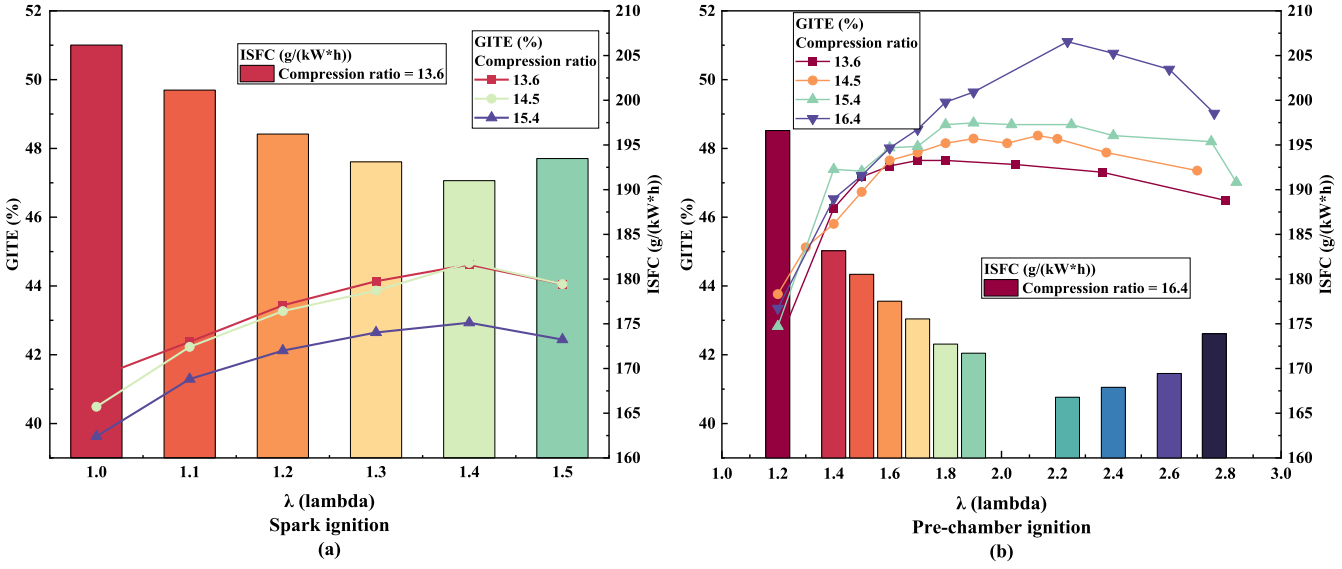

Figure 8. Effects of spark ignition and pre-chamber turbulent jet ignition on engine efficiency under different compression ratios.

Table 5. Case Setting

no.	ignition mode	compression ratio	lambda	spark time
Case 1	spark	13.6	1.4	−20
Case 2	spark	14.5	1.4	−16
Case 3	spark	15.4	1.4	−13
Case 4	Jet	13.6	1.8	−16
Case 5	Jet	14.5	2.13	−19.5
Case 6	Jet	15.4	2.25	−19
Case 7	Jet	16.4	2.236	−19.5

under higher compression ratios, the spark time must be decreased to maintain the engine's stability. In comparison to those of case 1, the GITE and ISFC of case 3 are significantly worse. For pre-chamber turbulent jet ignition, the ultra-lean mixture is less sensitive to knocking; therefore, even at a higher compression ratio, the spark timing rarely needs to be compromised and delayed, allowing the engine to operate at the optimal spark timing. The performance of the pre-chamber turbulent jet ignition is released, and at high compression ratios, the pre-chamber turbulent jet ignition has a more pronounced effect on engine performance.

Figure 10 compares the cylinder pressure, temperature, and rate of heat release between spark ignition and pre-chamber turbulent jet ignition under various compression ratios. The cylinder pressure depicted in Figure 10a correlates strongly with the compression ratio. As the compression ratio increases, spark ignition (cases 1−3) gradually decreases the peak cylinder pressure. With a higher compression ratio, the amount of charge per unit volume in the combustion chamber of the engine increases, and the peak cylinder pressure of the engine should have also increased. However, spark ignition must delay the ignition timing to ensure a stable engine operation (the impact of knocking), which shifts the combustion phase of the engine backward and reduces engine performance. Even at high compression ratios, the high knock tolerance of pre-chamber turbulent jet ignition keeps its combustion phasing in the optimal position; the cylinder pressure peak increases as the compression ratio increases.

https://doi.org/10.1021/acsomega.2c06810
ACS Omega 2023, 8, 4756−4766

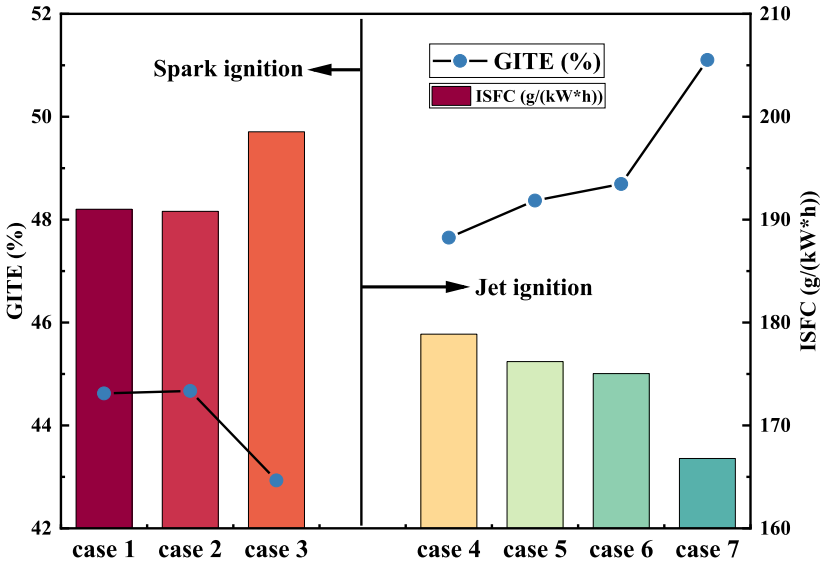

Figure 9. Comparison of the best GITE between spark ignition and pre-chamber turbulent jet ignition at different compression ratios.

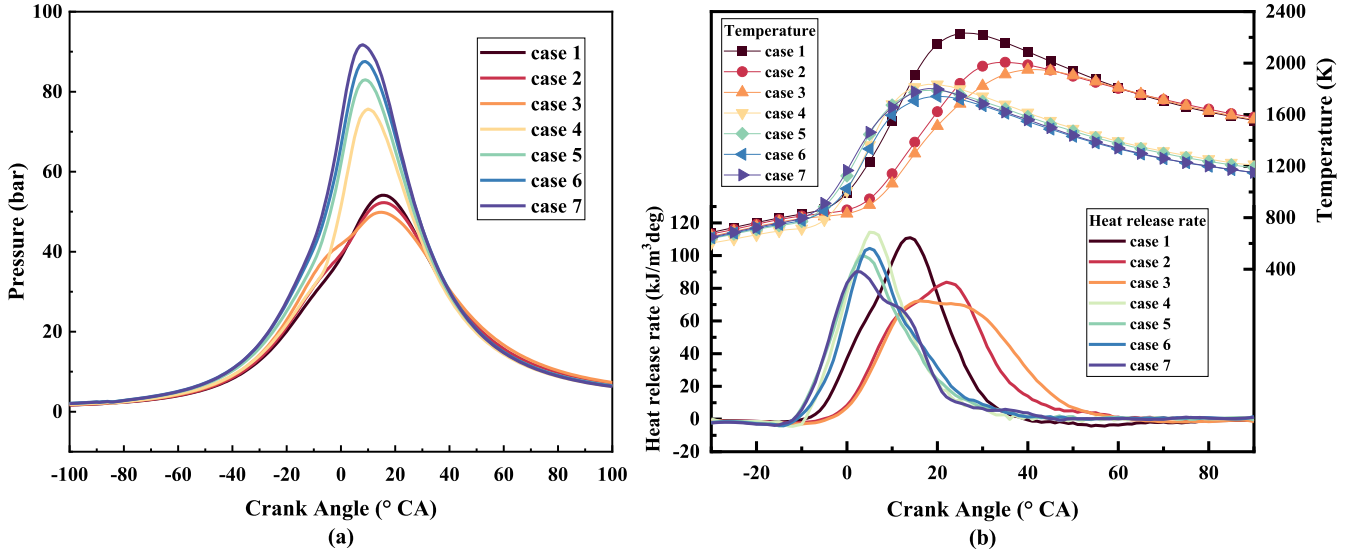

Figure 10. Comparison between spark ignition and pre-chamber turbulent jet ignition under typical conditions: (a) cylinder pressure comparison and (b) temperature and heat release rate comparison.

The view is further supported by Figure 10b, with the increasing compression ratio, which depicts an apparent and gradual decrease in the peak heat release rate for the same excess air coefficient for spark ignition (cases 1−3). The lean burn limit that sparks ignition can withstand is limited, so it is impossible to obtain better knock tolerance by increasing the intake air volume. Limited by the influence of the knock factor, the combustion process becomes less concentrated, and the temperature of the combustion decreases gradually. Unlike spark ignition, it can maintain an excellent level of combustion even at extremely high compression ratios. The peak heat release rate of pre-chamber injection ignition decreases as the compression ratio increases. In this instance, the engine pressure reduction effect caused by the decrease in the heat release rate is not as effective as the engine pressure increase caused by the different compression ratios, so the engine cylinder pressure remains elevated.

Figure 11 quantifies the engine's combustion process. CA10 begins with the spark timing and ends with the crankshaft

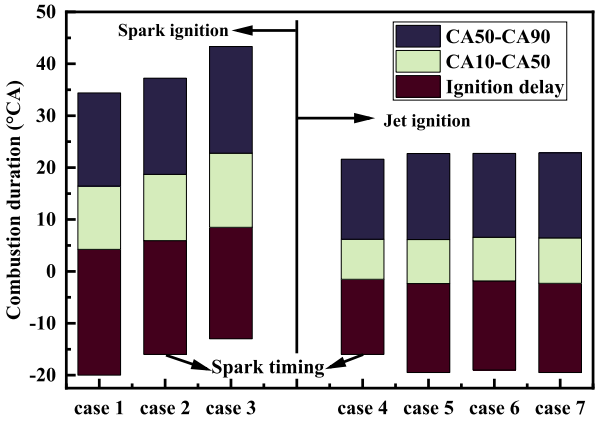

Figure 11. Comparison of the combustion process between spark ignition and pre-chamber turbulent jet ignition under typical conditions.

https://doi.org/10.1021/acsomega.2c06810
ACS Omega 2023, 8, 4756−4766

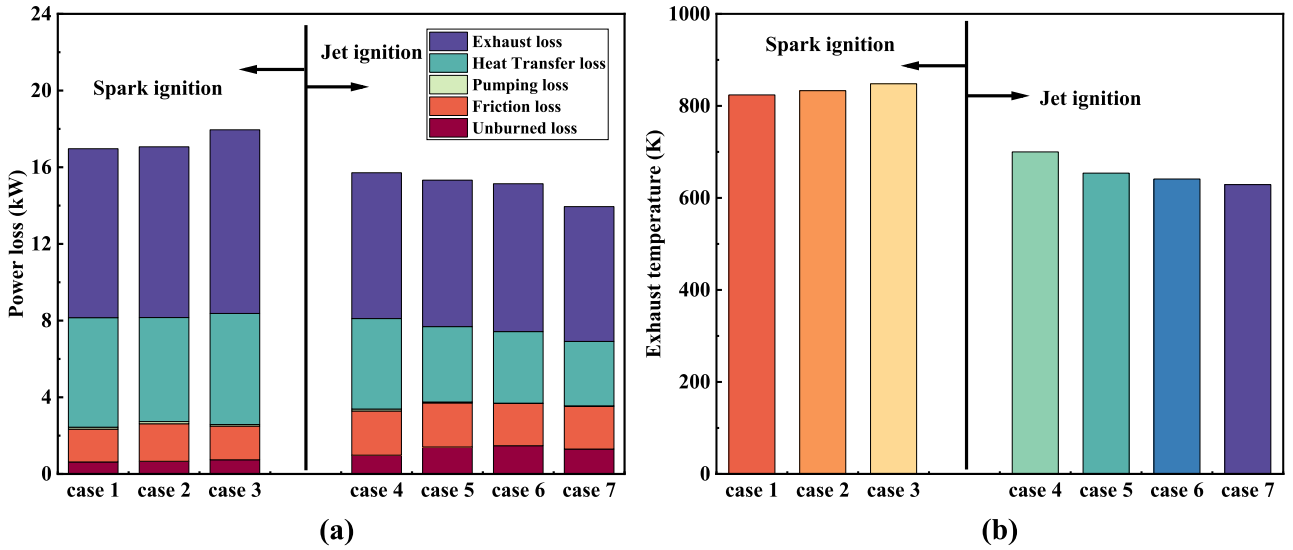

Figure 12. Comparison between spark ignition and pre-chamber turbulent jet ignition under typical conditions: (a) engine power loss comparison and (b) engine exhaust temperature comparison.

angle that corresponds to the 10% heat release of the engine fuel. Also, CA50 and CA90 behave similarly. The increased compression ratio does not retard the combustion phase of pre-chamber turbulent jet ignition compared to that of spark ignition, but there is a difference in the duration of combustion. At a low compression ratio, the mixture density and temperature per unit volume of the combustion chamber are lower, resulting in a slower rate of flame propagation. For case4, however, the optimal of the pre-chamber at a compression ratio of 13.6 is 1.8, and the lower excess air coefficient makes the flame acceleration effect brought about by the increase in compression less significant than the gain effect brought about by the higher mixture concentration. Therefore, the duration of combustion is reduced. In cases 5−7, although lambda continued to increase, the combustion duration was not significantly slowed, and the effect of the high compression ratio on further flame acceleration was evident.

Figure 12 compares the power losses and exhaust temperatures of spark ignition and turbulent jet ignition at various compression ratios. The power loss of spark ignition increases with the increase of the compression ratio, while the power loss of pre-chamber turbulent jet ignition decreases with the growth of the compression ratio.

The increase in unburned loss and heat transfer loss is the main reason for the increase of the spark ignition power loss at a high compression ratio. Affected by the knocking factor, the combustion phase of the spark ignition under a high compression ratio is significantly lagged, and it is difficult for the flame to quickly burn the mixture in the combustion chamber completely within a limited time. Also, the lag of the combustion phase makes the cylinder temperature lower near the compression top dead center, while the exhaust temperature is apparently increased, and a lot of heat is wasted in the engine exhaust gas. Therefore, the unburned loss and heat transfer loss are significantly increased.

The improved performance of pre-chamber turbulent jet ignition at high compression ratios is a result of the reduction of heat transfer and pump losses, as well as the modification of unburned losses. Under a high compression ratio, the effect of the cylinder's compression on the temperature increase is amplified. As the mixture's density increases, the rate of heat release accelerates during the early stages of combustion, resulting in a more concentrated heat release near the compression's top dead center; as a result, the heat is converted into mechanical energy with high efficiency. Consequently, the exhaust gas temperature decreases and heat transfer losses diminish. At high compression ratios, higher excess air coefficients are responsible for lower pump gas losses. A greater excess air coefficient results in an increased intake pressure and a decreased engine power consumption. The unburned losses are caused primarily by HC and CO in the exhaust gas, which will be discussed in greater detail in the following emission analysis.

Figure 13 illustrates the emission difference between spark ignition and pre-chamber turbulent jet ignition at various

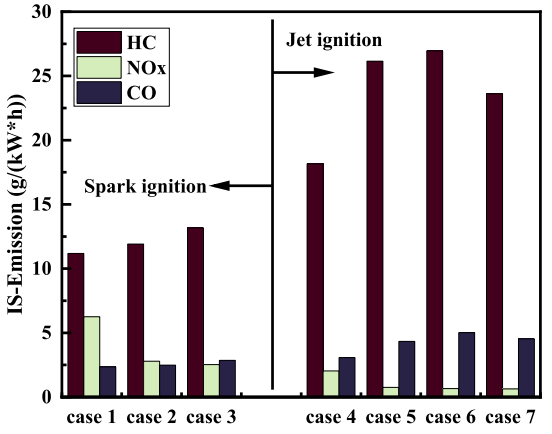

Figure 13. Emission comparison between spark ignition and pre-chamber turbulent jet ignition under typical conditions.

compression ratios. Not only does spark ignition reduce the engine efficiency at high compression ratios but it also worsens engine emissions. As shown in Figure 10b, as the compression ratio increases, the in-cylinder temperature in the combustion process of spark ignition decreases significantly due to the influence of the knock factor. The decrease in cylinder temperature leads to a significant decrease in the forward reaction rate of HC and a significant increase in HC emissions.

https://doi.org/10.1021/acsomega.2c06810
ACS Omega 2023, 8, 4756−4766

Two conditions are required for the creation of NOx: high temperature and oxygen enrichment. At high compression ratios, the large drop in cylinder temperature under the spark ignition operating conditions of case 1−3 reduces NOx emissions. Under a high compression ratio, the HC emission of the pre-chamber turbulent jet ignition exhibited an upward trend and then a downward trend. This is due to the fact that at higher compression ratios, the engine's optimal lambda gradually increases, causing the HC emission to increase while the NOx emission gradually decreases. At the same time, the high compression ratio increases the amount of the mixture in the pre-chamber, which increases the energy and intensity of the turbulent jet in the pre-chamber and accelerates the combustion process in the main chamber, which prevents the burn duration from being prolonged even at a higher compression ratio. In addition, the compression ratio in this article is adjusted by the cylinder gasket, and the clearance volume at the cylinder gasket is decreased at higher compression ratios, resulting in a reduction in HC emissions at high compression ratios.

4. CONCLUSIONS

I In this paper, a high compression ratio ultra-lean burn is achieved by applying pre-chamber turbulent jet ignition to a single-cylinder AVL5400 Miller engine, and the performance difference between spark ignition and pre-chamber turbulent jet ignition of a high compression ratio is compared. The key findings are as follows.

1. Pre-chamber turbulent jet ignition can significantly extend the lean burn limit of spark ignition engines, enhancing the engine efficiency and decreasing NOx emissions. Under ultra-lean conditions, however, CO and HC emissions increase. Due to the high combustion speed and potent ignition capability of the pre-chamber turbulent jet ignition, the engine is able to run steadily under ultra-lean conditions, resulting in the economic improvement. This causes a significant change in the structure of the engine's power loss, with an increase in unburned losses but a significant decrease in heat transfer losses and pump gas losses to deficient levels.
2. With the compression ratio increase, the pre-chamber turbulent jet ignition economy improvement becomes more pronounced while the spark ignition deteriorates. When the compression ratio is 16.4 and λ = 2.236, the engine economy reaches a global optimum with a GITE of 51.10% and an ISFC of 166.78 g/kWh.
3. The pre-chamber turbulent jet ignition is not sensitive to knocking because it can operate stably under ultra-lean conditions, and the MBT can always be maintained at the optimal level. The higher compression ratio brings forward the earlier heat release of the turbulent jet ignition, and the optimum λ of the engine increases gradually.
4. In terms of the power loss structure, the improvement in pre-chamber turbulent jet ignition engine performance at high compression ratios is primarily attributable to the higher indicated work output due to higher cylinder pressure and the significant reduction in heat transfer losses, where the residual energy in the engine exhaust gas is significantly reduced and the exhaust temperature is only about 350 °C.

AUTHOR INFORMATION

Corresponding Author

Jiakun Du − *GAC Automotive Research & Development Center, Guangzhou 511434 Guangdong, People's Republic of China;* orcid.org/0000-0003-4769-3361; Email: dujiakun@gacrnd.com

Authors

Wenfeng Zhan − *School of Mechanical & Automotive Engineering, South China University of Technology, Guangzhou 510640, People's Republic of China; GAC Automotive Research & Development Center, Guangzhou 511434 Guangdong, People's Republic of China*

Hong Chen − *GAC Automotive Research & Development Center, Guangzhou 511434 Guangdong, People's Republic of China*

Bin Wang − *College of Automotive Engineering, Jilin University, Changchun 130025, People's Republic of China*

Fangxi Xie − *College of Automotive Engineering, Jilin University, Changchun 130025, People's Republic of China;* orcid.org/0000-0002-4968-4584

Yuhuai Li − *GAC Automotive Research & Development Center, Guangzhou 511434 Guangdong, People's Republic of China*

Complete contact information is available at: https://pubs.acs.org/10.1021/acsomega.2c06810

Author Contributions

Conceptualization, J.D. and H.C.; methodology, J.D and F.X.; validation, J.D. and F.X.; formal analysis, W.Z. and B.W.; investigation, W.Z. and H.C.; resources, Y.L.; data curation, Y.L.; writing—original draft preparation, W.Z.; and writing—review and editing, W.Z. and B.W. All authors have read and agreed to the published version of the manuscript.

Notes

The authors declare no competing financial interest.

ACKNOWLEDGMENTS

This work was supported financially by the Performance Optimization of Multi-Mode Drive Plug-in Passenger Vehicles, a key project of the Ministry of Science and Technology of the People's Republic of China (2017yFB0103300).

REFERENCES

(1) Liu, Z.; Hao, H.; Cheng, X.; Zhao, F. Critical Issues of Energy Efficient and New Energy Vehicles Development in China. *Energy Policy* **2018**, *115*, 92−97.

(2) Xiao, B.; Ruan, J.; Yang, W.; Walker, P. D.; Zhang, N. A Review of Pivotal Energy Management Strategies for Extended Range Electric Vehicles. *Renew. Sustain. Energy Rev.* **2021**, *149*, 111194.

(3) Lan, S.; Stobart, R.; Wang, X. Matching and Optimization for a Thermoelectric Generator Applied in an Extended-Range Electric Vehicle for Waste Heat Recovery. *Appl. Energy* **2022**, *313*, 118783.

(4) Oh, H.; Bae, C. Effects of the Injection Timing on Spray and Combustion Characteristics in a Spray-Guided DISI Engine under Lean-Stratified Operation. *Fuel* **2013**, *107*, 225−235.

(5) Gong, C.; Li, Z.; Sun, J.; Liu, F. Evaluation on Combustion and Lean-Burn Limit of a Medium Compression Ratio Hydrogen/Methanol Dual-Injection Spark-Ignition Engine under Methanol Late-Injection. *Appl. Energy* **2020**, *277*, 115622.

(6) Chen, Z.; Wang, L.; Zhang, Q.; Zhang, X.; Yang, B.; Zeng, K. Effects of Spark Timing and Methanol Addition on Combustion Characteristics and Emissions of Dual-Fuel Engine Fuelled with

https://doi.org/10.1021/acsomega.2c06810
ACS Omega 2023, 8, 4756−4766

Natural Gas and Methanol under Lean-Burn Condition. *Energy Convers. Manag.* **2019**, *181*, 519−527.
(7) Duan, X.; Li, Y.; Liu, J.; Guo, G.; Fu, J.; Zhang, Q.; Zhang, S.; Liu, W. Experimental Study the Effects of Various Compression Ratios and Spark Timing on Performance and Emission of a Lean-Burn Heavy-Duty Spark Ignition Engine Fueled with Methane Gas and Hydrogen Blends. *Energy* **2019**, *169*, 558−571.
(8) Wang, B.; Xie, F.; Hong, W.; Du, J.; Chen, H.; Su, Y. The Effect of Structural Parameters of Pre-Chamber with Turbulent Jet Ignition System on Combustion Characteristics of Methanol-Air Pre-Mixture. *Energy Convers. Manag.* **2022**, *274*, 116473.
(9) Gong, C.; Yi, L.; Zhang, Z.; Sun, J.; Liu, F. Assessment of Ultra-Lean Burn Characteristics for a Stratified-Charge Direct-Injection Spark-Ignition Methanol Engine under Different High Compression Ratios. *Appl. Energy* **2020**, *261*, 114478.
(10) Jung, D.; Sasaki, K.; Sugata, K.; Matsuda, M.; Yokomori, T.; Iida, N.Combined Effects of Spark Discharge Pattern and Tumble Level on Cycle-to-Cycle Variations of Combustion at Lean Limits of SI Engine Operation. *SAE Tech. Pap.***2017**, *2017*. (March). DOI: 10.4271/2017-01-0677.
(11) Chen, L.; Wei, H.; Zhang, R.; Pan, J.; Zhou, L.; Feng, D. Effects of Spark Plug Type and Ignition Energy on Combustion Performance in an Optical SI Engine Fueled with Methane. *Appl. Therm. Eng.* **2019**, *148*, 188−195.
(12) Gong, C.; Zhang, Z.; Sun, J.; Liu, F. Optimization on Timings of Injection and Spark of a High Compression-Ratio Stratified-Charge Methanol Engine under Ultra-Lean Burn. *Fuel* **2021**, *285*, 119227.
(13) Hua, J.; Song, Y.; Zhou, L.; Liu, F.; Wei, H. Operation Strategy Optimization of Lean Combustion Using Turbulent Jet Ignition at Different Engine Loads. *Appl. Energy* **2021**, *302*, 117586.
(14) Biswas, S.; Tanvir, S.; Wang, H.; Qiao, L. On Ignition Mechanisms of Premixed CH4/Air and H2/Air Using a Hot Turbulent Jet Generated by Pre-Chamber Combustion. *Appl. Therm. Eng.* **2016**, *106*, 925−937.
(15) Gholamisheeri, M.; Wichman, I. S.; Toulson, E. A Study of the Turbulent Jet Flow Field in a Methane Fueled Turbulent Jet Ignition (TJI) System. *Combust. Flame* **2017**, *183*, 194−206.
(16) Qin, F.; Shah, A.; Huang, Z.; Peng, L.; Tunestal, P.; Bai, X. S. Detailed Numerical Simulation of Transient Mixing and Combustion of Premixed Methane/Air Mixtures in a Pre-Chamber/Main-Chamber System Relevant to Internal Combustion Engines. *Combust. Flame* **2018**, *188*, 357−366.
(17) Li, Y.; Luo, H.; Gao, W.; Chen, H.; Zhan, W.; Du, J. Effects of Combustion and Emissions of Turbulent Jet Ignition with a Small-Volume Prechamber for a Gasoline Engine. *J. Energy Eng.* **2022**, *148*, 1−10.
(18) Korb, B.; Kuppa, K.; Nguyen, H. D.; Dinkelacker, F.; Wachtmeister, G. Experimental and Numerical Investigations of Charge Motion and Combustion in Lean-Burn Natural Gas Engines. *Combust. Flame* **2020**, *212*, 309−322.
(19) Zhou, L.; Liu, P.; Zhong, L.; Feng, Z.; Wei, H. Experimental Observation of Lean Flammability Limits Using Turbulent Jet Ignition with Auxiliary Hydrogen and Methane in Pre-Chamber. *Fuel* **2021**, *305*, 121570.
(20) Zhao, Z.; Wang, Z.; Qi, Y.; Cai, K.; Li, F. Experimental Study of Combustion Strategy for Jet Ignition on a Natural Gas Engine. *Int. J. Engine Res.* **2022**, *23*, 104−119.
(21) Hua, J.; Zhou, L.; Gao, Q.; Feng, Z.; Wei, H. Influence of Pre-Chamber Structure and Injection Parameters on Engine Performance and Combustion Characteristics in a Turbulent Jet Ignition (TJI) Engine. *Fuel* **2021**, *283*, 119236.
(22) Bunce, M.; Blaxill, H.Sub-200 g/KWh BSFC on a Light Duty Gasoline Engine. *SAE Tech. Pap***2016**, *2016*(). DOI: 10.4271/2016-01-0709.
(23) Attard, W. P.; Toulson, E.; Huisjen, A.; Chen, X.; Zhu, G.; Schock, H. Spark Ignition and Pre-Chamber Turbulent Jet Ignition Combustion Visualization. *SAE Tech. Pap.* **2012**, DOI: 10.4271/2012-01-0823.
(24) Attard, W. P.; Kohn, J.; Parsons, P. Ignition Energy Development for a Spark Initiated Combustion System Capable of High Load, High Efficiency and near Zero NOx Emissions. *SAE Tech. Pap.* **2010**, *3*, 481−496.
(25) Attard, W. P.; Blaxill, H. A Single Fuel Pre-Chamber Jet Ignition Powertrain Achieving High Load, High Efficiency and near Zero NOx Emissions. *SAE Tech. Pap.* **2011**, *5*, 734−746.
(26) Attard, W. P.; Blaxill, H.; Anderson, E. K.; Litke, P. Knock Limit Extension with a Gasoline Fueled Pre-Chamber Jet Igniter in a Modern Vehicle Powertrain. *SAE Int. J. Engines* **2012**, *5*, 1201−1215.
(27) Shah, A.; Tunestal, P.; Johansson, B.Effect of Relative Mixture Strength on Performance of Divided Chamber "Avalanche Activated Combustion" Ignition Technique in a Heavy Duty Natural Gas Engine. *SAE Tech. Pap.***2014**, *1*. DOI: 10.4271/2014-01-1327.
(28) Tang, Q.; Jiang, P.; Peng, C.; Duan, X.; Zhao, Z. Impact of Acetone−Butanol−Ethanol (ABE) and Gasoline Blends on the Energy Balance of a High-Speed Spark-Ignition Engine. *Appl. Therm. Eng.* **2021**, *184*, 116267.
(29) Gholamisheeri, M.; Givler, S.; Toulson, E. Large Eddy Simulation of a Homogeneously Charged Turbulent Jet Ignition System. *Int. J. Engine Res.* **2019**, *20*, 181−193.

https://doi.org/10.1021/acsomega.2c06810
ACS Omega 2023, 8, 4756−4766